

## GRB 070306: A HIGHLY EXTINGUISHED AFTERGLOW<sup>1</sup>

A. O. JAUNSEN,<sup>2</sup> E. ROL,<sup>3</sup> D. J. WATSON, D. MALESANI, J. P. U. FYNBO, B. MILVANG-JENSEN, J. HJORTH, P. M. VREESWIJK,<sup>4</sup> J.-E. OVALDSEN,<sup>2</sup> K. WIERSEMA, N. R. TANVIR,<sup>3</sup> J. GOROSABEL,<sup>5</sup> A. J. LEVAN,<sup>6</sup> M. SCHIRMER,<sup>7</sup> AND A. J. CASTRO-TIRADO<sup>5</sup>

Received 2007 November 30; accepted 2008 March 26

### ABSTRACT

We report on the highly extinguished afterglow of GRB 070306 and the properties of the host galaxy. An optical afterglow was not detected at the location of the burst, but in near-infrared a doubling in brightness during the first night and later power-law decay in the  $K$  band provided a clear detection of the afterglow. The host galaxy is relatively bright,  $R \sim 22.8$ . An optical low-resolution spectrum revealed a largely featureless host galaxy continuum with a single emission line. Higher resolution follow-up spectroscopy shows this emission to be resolved and consisting of two peaks separated by  $7 \text{ \AA}$ , suggesting it to be  $[\text{O II}]$  at a redshift of  $z = 1.49594 \pm 0.00006$ . The infrared color  $H - K = 2$  directly reveals significant reddening. By modeling the optical/X-ray spectral energy distribution at  $t = 1.38$  days with an extinguished synchrotron spectrum, we derive  $A_V = 5.5 \pm 0.6$  mag. This is among the largest values ever measured for a GRB afterglow, and visual extinctions exceeding unity are rare. The importance of early near-IR observations is obvious and may soon provide a clearer view into the once elusive “dark bursts.”

*Subject headings:* dust, extinction — gamma rays: bursts

### 1. INTRODUCTION

Long gamma-ray bursts (GRBs) are believed to be indicators of star formation due to their association with short-lived massive stars (Galama et al. 1998; Hjorth et al. 2003; Stanek et al. 2003). These events should therefore offer great prospects for characterizing the star formation history of the universe (Wijers et al. 1998), as GRBs can be detected (in gamma and X-rays) at all observable redshifts and through large columns of dust and gas. One potential objection to this is if GRBs are biased toward a special subset of massive stars, i.e., those of low metallicity or in peculiar circumstellar environments. On the other hand, if there is no dependency on metallicity, then the nature of the host galaxies leads to the surprising conclusion that most stars are formed in dwarf galaxies (Fynbo et al. 2008).

In the pre-*Swift* era the detection of optical afterglows (OAs) was a requirement for subarcsecond localizations. This was obtained for about 30% of the GRBs due to effects such as observability, weather conditions, and so on. However, in a few cases stringent upper limits on the early (optical) afterglow could be obtained (see, e.g., Groot et al. 1998), providing evidence for a subclass of OA-less bursts dubbed “dark bursts” (see, e.g., Fruchter 1999; Lamb & Reichart 2000; Fynbo et al. 2001; Berger et al.

2002; Lazzati et al. 2002a). Today the situation is quite different as the majority of bursts (>90%) are localized with the *Swift* XRT instrument (Gehrels et al. 2004; Burrows et al. 2005). Jakobsson et al. (2004) proposed an unbiased definition of a dark burst by suggesting that the spectral slope between the optical and X-ray is  $\beta_{\text{ox}} < 0.5$ . As many as 25% of the *Swift* bursts fulfill this criterion (Fynbo et al. 2008). Throughout the paper we adopt this definition of a dark burst. There are several effects that may cause an afterglow to be classified as dark, but among the most obvious and possibly dominant effects are dust obscuration and high redshift (see also Roming et al. 2006).

Although the afterglows of dark bursts do not all go by undetected, there is a sizeable subclass of bursts for which we do not have much information, and these may consequently affect the luminosity function and statistics of GRBs and their host galaxies significantly (see, e.g., Rol et al. 2007b, who reported on a dark burst with significant extinction). There are also a few systems which do not resemble the general population of GRBs (Perley et al. 2008).

In this paper we present the detection of the NIR afterglow of GRB 070306 which is characterized as a dark burst. The most likely interpretation is that the afterglow is heavily dust obscured and the level of extinction provides a unique opportunity to study the local dust properties of the progenitor. The outline of this paper is as follows: In § 2 we describe the *Swift* X-ray data, and our optical and near-infrared observations of GRB 070306. The host and the spectral energy distribution (SED) template fitting is described in § 3, the afterglow and the extinction curve fits are discussed in § 4, while the results are summarized and discussed in § 5.

Throughout the paper we assume a cosmology with  $H_0 = 70 \text{ km s}^{-1} \text{ Mpc}^{-1}$ ,  $\Omega_M = 0.3$ , and  $\Omega_\Lambda = 0.7$ . The afterglow is characterized by a standard temporal and spectral power law of the form,  $F_\nu \propto t^{-\alpha} \nu^{-\beta}$ . All quoted errors are  $1 \sigma$  (68%), unless noted differently.

### 2. OBSERVATIONS AND REDUCTIONS

GRB 070306 was discovered by *Swift* at ( $t_0$ ) 16:44:28.0 UT on 2007 March 6 (Pandey et al. 2007). The burst had a

<sup>1</sup> Based on observations made at the European Southern Observatory, Paranal, Chile under programs 078.D-0416, 177.A-0591; with the Nordic Optical Telescope, operated on the island of La Palma jointly by Denmark, Finland, Iceland, Norway, and Sweden in the Spanish Observatorio del Roque de los Muchachos of the Instituto de Astrofísica de Canarias; and with the William Herschel Telescope operated on the island of La Palma by the Isaac Newton Group in the Spanish Observatorio del Roque de los Muchachos of the Instituto de Astrofísica de Canarias.

<sup>2</sup> Institute of Theoretical Astrophysics, University of Oslo, PO Box 1029 Blindern, N-0315 Oslo, Norway.

<sup>3</sup> Department of Physics and Astronomy, University of Leicester, Leicester, LE1 7RH, UK.

<sup>4</sup> Dark Cosmology Centre, Niels Bohr Institute, University of Copenhagen, Juliane Maries Vej 30, DK-2100 Copenhagen, Denmark.

<sup>5</sup> Instituto de Astrofísica de Andalucía (IAA-CSIC), Aparado de Correos 3004, Granada, Spain.

<sup>6</sup> Department of Physics, University of Warwick, Coventry, CV4 7AL, UK.

<sup>7</sup> Isaac Newton Group of Telescopes (INT), Apartado de Correos 321, 38700 Santa Cruz de La Palma, Tenerife, Spain.

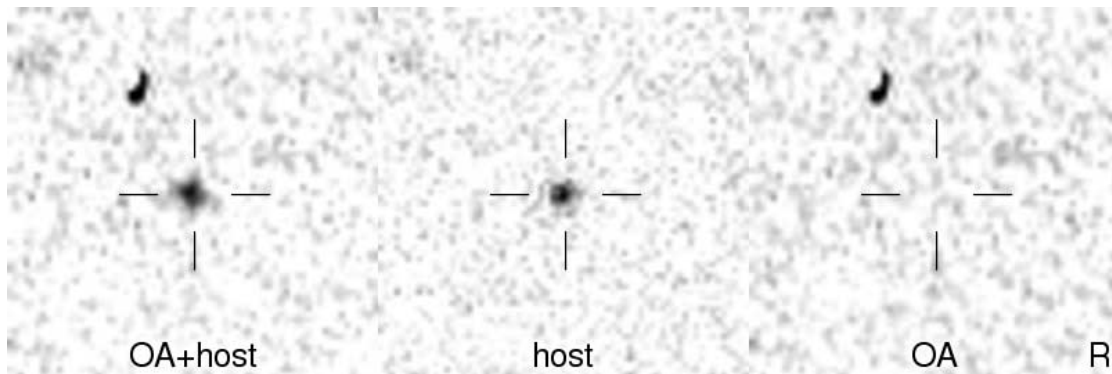


FIG. 1.— $R$ -band image at March 08.10 (*left*), combined April 20 and May 7 (*middle*) and the difference image (*right*) obtained using ISIS. No residual emission is detected and the estimated upper limit of the afterglow is  $R > 23.5$  (estimated as described in § 2.2.1). North is up, and east is left.

$T_{90} = 210 \pm 10$  s (Barthelmy et al. 2007). *Swift* slewed immediately, and XRT observations began at  $t_0 + 153$  s and with UVOT at  $t_0 + 162$  s. An X-ray afterglow was identified and reported by Page & Pandey (2007).

### 2.1. X-Ray

The *Swift* XRT light curve shows a typical plateau phase, ending at approximately 35 ks after the BAT trigger. To produce the X-ray spectrum at the time of the optical observations, the PC events after the plateau phase (35–266 ks) were reduced in a standard way using the most recent calibration data and normalized to the count rate at the time of the optical observations ( $t_0 + 1.38$  days). A power law with fixed Galactic and variable absorption at the redshift of the host ( $z = 1.4959$ ; see §§ 3 and 4) fits the data well ( $\chi^2/\text{dof} = 27.1/31$ ). The best-fit photon index  $\Gamma = 2.2 \pm 0.1$  ( $\beta_X = 1.2 \pm 0.1$ ); the excess absorption  $N_{\text{H}} = (2.6 \pm 0.4) \times 10^{22} \text{ cm}^{-2}$  for the equivalent hydrogen column density (assuming solar abundances), in excess of the Galactic value ( $3 \times 10^{20} \text{ cm}^{-2}$ ; Dickey & Lockman 1990) corresponding to  $(0.4 \pm 0.04) \times 10^{22} \text{ cm}^{-2}$  at  $z = 0$ . We note that the fit with excess absorption at  $z = 0$  is poor. For subsolar ( $Z = 0.1 Z_{\odot}$ ) metallicity we find  $N_{\text{H}} = (20 \pm 3) \times 10^{22} \text{ cm}^{-2}$ . There is no evidence for a change in the spectral parameters between the plateau and postplateau phases: the best-fit absorption and spectral slope parameters were consistent to within  $1 \sigma$ .

The optical to X-ray spectral slope can be estimated at March 07.00 UT by using the specific 3 keV flux at this time ( $0.79 \mu\text{Jy}$ ) and the estimated upper limit on the afterglow from the  $I$ -band Nordic Optical Telescope (NOT) image at March 06.95 UT [ $I > 22$  mag (Vega), or  $F_{\nu} < 4.1 \mu\text{Jy}$ ]. This gives an upper limit of  $\beta_{\text{ox}} < 0.23$ . This is, hence, a dark burst according to the definition of Jakobsson et al. (2004,) which requires that  $\beta_{\text{ox}} < 0.5$ .

### 2.2. Optical and Near-Infrared

We carried out early follow-up to localize the afterglow in the optical using the 2.5 m Nordic Optical Telescope and ALFOSC instrument and in the near-infrared using the 4.2 m William Herschel Telescope (WHT) and LIRIS instrument on Observatorio del Roque de los Muchachos. Observing conditions were good, but the Moon was close to being full. Imaging and photometry data from the SDSS (Cool et al. 2007) revealed an object close to the detection limit within the error circle. Initial observations did not reveal an afterglow (Uemura et al. 2007), but Rol et al. (2007a) reported the detection of a fairly bright near-infrared (NIR) afterglow detected 3.3 hr after the burst which 4.7 hr later had brightened by nearly a factor of 2 (Levan et al. 2007). The NIR afterglow was consistent with the location of the optical SDSS detection. Optical

follow-up detected an object consistent in location and brightness with the object seen in the SDSS data (Malesani et al. 2007). The NIR follow-up was continued the following night when we triggered target-of-opportunity (ToO) observations with VLT ISAAC under program 078.D-0416(E) (PI: Vreeswijk). A FORS 200V optical spectrum was obtained [program ID 078.D-0416(B)] at the position of the NIR afterglow and optical SDSS detection in order to secure a redshift measurement. A second ISAAC epoch was obtained on the following night to further characterize the NIR afterglow. Unfortunately, continued follow-up was not possible as all available time for this run had been exhausted. Finally, late-time NIR observations to secure estimates of the host were obtained with the WHT LIRIS in the end of April and a  $K$ -band point in January 2008 as part of a GRB host program at VLT ISAAC [program ID 177.A-0591(Q); PI: J. Hjorth].

Using our best optical  $R$ -band image and 30 objects from the USNO B1.0 catalog, we determine the location of the host galaxy to be  $(\alpha, \delta) = (09^{\text{h}}52^{\text{m}}23.30^{\text{s}} \pm 0.20^{\text{s}}, +10^{\circ}28'55.5'' \pm 0.12'')$ . Images of the GRB afterglow and host in  $R$  and  $K$  band are shown in Figures 1 and 2. The afterglow in the  $K$  band has the same location within the errors, although a small offset of not more than a pixel ( $0.15''$ ) can be seen in Figure 2. The host galaxy appears pointlike in most of the filters, with the exception of the  $K$  band, where the deeper image reveals some faint extended emission.

#### 2.2.1. Imaging

The optical data were processed in the standard way using IRAF<sup>8</sup> and packages therein. The near-infrared data were processed using a combination of observatory pipelines (Eclipse, THELI) and IDL. Absolute photometric calibration was performed on the best available imaging data ( $R$  on May 7,  $I$  on March 12, and NIR on March 9) using SExtractor (Bertin & Arnouts 1996) and a fixed aperture of  $3.0''$  radius. The zero point was established from standard star observations for the NIR (ISAAC) data, while for the FORS and NOT (optical) data we used six field stars from the SDSS data to photometrically calibrate our  $R$  and  $I$  bands using the color transformations of Jester et al. (2005). The remaining observations were calibrated by offsetting the photometry relative to these reference images. The results are given in Table 1, and the reference images are denoted by asterisks. The foreground reddening is estimated to  $E(B - V) = 0.0275$  using the maps of Schlegel et al. (1998) but the column containing afterglow (Vega) magnitudes given in Table 1 have not been corrected for the Galactic extinction.

<sup>8</sup> Image Reduction and Analysis Facility (IRAF), a software system distributed by the National Optical Astronomy Observatory (NOAO).

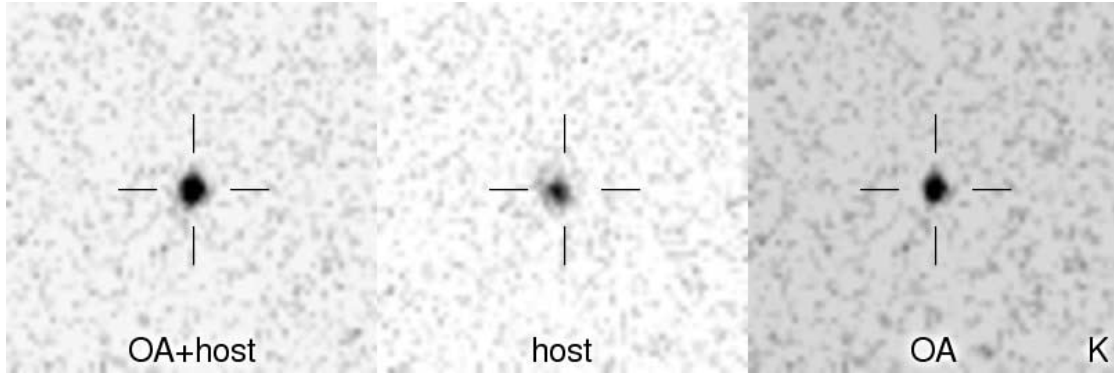


FIG. 2.—Image subtraction (ISIS) is used to detect variability, and in this montage we show the  $K$ - and image of March 08.21 with contribution from the afterglow and host (*left*). In the middle frame the late-time (host) image from 2008 January 30.22 is shown, clearly revealing its extended nature. To the right the difference image reveals the significant contribution of the afterglow of GRB 070306 in the  $K$  band. The images, which have been registered using field stars, show that the afterglow is centered on the brightest region in the host galaxy (although a small offset toward the northwest may be present on the order of a pixel,  $0.15''$ ). North is up, and east is left.

Optimal sensitivity to variability is achieved by degrading each frame to the worst PSF quality in a series of images (for a given filter). The difference images are then inspected to identify residual emission at the afterglow position. We performed image subtraction using the ISIS package (Alard & Lupton 1998) on all relevant imaging data. The reference frame for each filter (for registration and flux variability) was generally chosen as the latest epoch, but for  $J$  and  $H$  band these frames had a very low signal-to-noise ratio and produced very poor image-subtracted results. For these two series an earlier epoch had to be selected as a reference, although this was not ideal due to a possible afterglow contribution. The actual reference frames are indicated in Table 1. Prior to running ISIS, the images were registered and transformed using the IRAF `immatch` package in order to ensure a common coordinate system and smooth processing by ISIS. We also copied an isolated star (a pseudo PSF) of similar flux as that of the afterglow

to an empty region of sky near the location of the GRB so that it would remain in the field after the image subtraction (for comparison purposes). In those frames for which we detected a residual ( $2\sigma$  level) at the location of the GRB we employed fixed aperture photometry (using SExtractor) and an aperture radius of  $1.5''$  to measure the relative flux between the residual and the reference star. In the opposite case, in which no residual (at the  $2\sigma$  level) could be detected, we estimated the detection limit by scaling our chosen PSF star by a decreasing amount and placing it at the location of the GRB afterglow/host. Image subtraction was then performed as described earlier and the magnitude difference was computed relative to the reference star (pseudo PSF). This process was repeated until it could no longer be detected, determining the afterglow detection limit (or upper limit).

The multicolor light curve ( $J, H, K$  bands) is shown in Figure 3 and is characterized by an initial rise to peak during the first day in

TABLE 1  
OBSERVING LOG AND RESULTS FROM PHOTOMETRY

Date (UT)	Time <sup>a</sup> (day)	Instrument	Band	Seeing (arcsec)	$T_{\text{int}}$ (s)	Vega Magnitude <sup>b</sup>	Error (mag)	$F_{\nu}$ <sup>c</sup> ( $\mu\text{Jy}$ )	Error ( $\mu\text{Jy}$ )
Mar 06.8889.....	0.191	WHT LIRIS	$J$	1.1	1200	>22.4	...	<1.7	...
Mar 08.0542.....	1.357	VLT ISAAC	$J$	0.9	1040	>22.0	...	<2.5	...
Mar 09.2342.....	2.537	VLT ISAAC	$J$	0.7	2560	(20.90)*	0.13	6.82	0.75
Apr 30.8871.....	55.190	WHT LIRIS	$J$	0.8	1800	...	...	...	...
Mar 06.8670.....	0.170	WHT LIRIS	$H$	1.1	1200	19.78	0.12	12.31	1.36
Mar 08.0836.....	1.386	VLT ISAAC	$H$	0.8	1152	20.52	0.21	6.23	1.20
Mar 09.2074.....	2.510	VLT ISAAC	$H$	0.6	1344	(20.00)*	0.20	10.05	1.48
Apr 30.9242.....	55.227	WHT LIRIS	$H$	1.0	1800	...	...	...	...
Mar 06.8416.....	0.144	WHT LIRIS	$K$	1.0	1500	18.28	0.15	31.92	4.41
Mar 07.0361.....	0.339	WHT LIRIS	$K$	0.9	1200	17.61	0.14	59.16	7.62
Mar 08.0701.....	1.373	VLT ISAAC	$K$	0.7	1152	18.53	0.15	25.35	3.50
Mar 08.2153.....	1.512	VLT ISAAC	$K$	0.6	1152	18.50	0.15	26.06	3.60
Mar 09.1879.....	2.490	VLT ISAAC	$K$	0.6	1152	19.83	0.19	7.66	1.34
Apr 30.9699.....	55.272	WHT LIRIS	$K$	0.9	1800	...	...	...	...
Jan 30.2244.....	329.526	VLT ISAAC	$K$	0.5	1920	(19.60)*	0.19	...	...
Mar 06.9523.....	0.255	NOT StanCam	$I$	1.0	1200	...	...	...	...
Mar 12.0615.....	5.364	NOT ALFOC	$I$	0.6	3600	(22.15)*	0.19	3.57	0.62
Mar 08.1042.....	1.407	VLT FORS2	$R$	0.9	120	>23.5	...	<1.3	...
Apr 20.0507.....	44.364	VLT FORS2	$R$	0.9	180	>23.5	...	<1.3	...
May 07.0040.....	61.306	VLT FORS2	$R$	0.7	60	(22.78)*	0.23	2.53	0.54

<sup>a</sup> Time since burst trigger  $t_0 = 2007 \text{ Mar } 6.6976 \text{ UT}$ .

<sup>b</sup> The photometry was obtained by measuring the flux in circular apertures of  $3.0''$  radius (using SExtractor) on the best data available (around March 9.2,  $t = 1.38$  days and best in terms of subarcsecond seeing, photometric conditions, and telescope aperture). All other magnitudes and upper limits are measured from image-subtracted frames and calibrated using the reference frames, which are identified by the asterisks (see § 2.2.1 for details). Entries with no value in this column are due to inferior data quality of the observation in comparison to the reference images and the host itself was only marginally detected.

<sup>c</sup> The flux values have been computed using the AB offsets (see § 4) and correcting for Galactic extinction according to Schlegel et al. (1998).

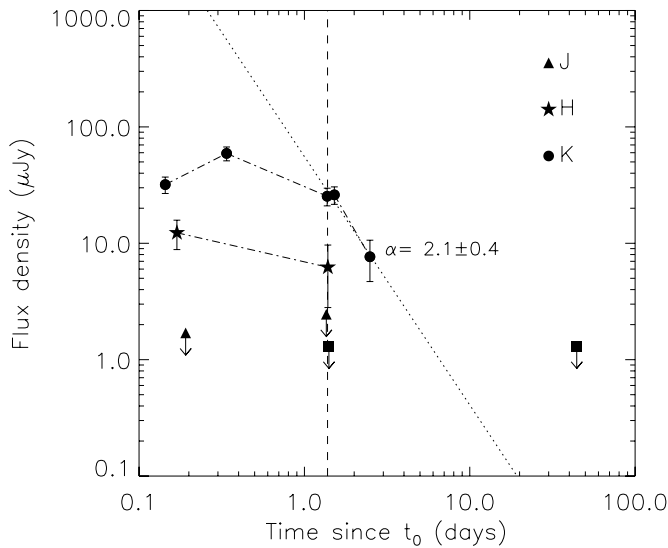


FIG. 3.—Multicolor light curve ( $J$ ,  $H$ ,  $K$ ) of GRB 070306 and estimated late-time decay index,  $\alpha = 2.1 \pm 0.4$ . The vertical dashed line marks the simultaneity time,  $t_0 + 1.38$  days. Upper limits are denoted by an arrow.

the  $K$  band and possibly also in the  $H$  band. The subsequent decline can be approximated by a power law,  $F \propto t^{-\alpha}$ . During the second and third days we fit the power-law decline in the  $K$  band with  $\alpha = 2.1 \pm 0.4$  typical for postbreak light curves (e.g., Andersen et al. 2000, their Fig. 4). No slope could be measured for the  $J$  and  $H$  bands. In the  $H$  band the afterglow is clearly detected in the first two epochs, but the poorer image quality and lower signal-to-noise ratio of the last epoch prevented us from setting meaningful limits on the earlier epochs and we were therefore forced to use the third epoch as a reference image. In addition, the images originate from two different instruments, which clearly does not help. Consequently, we are unable to detect an afterglow component at this epoch and may possibly overestimate the flux of the host (if there is a detectable contribution from the afterglow in this third epoch). We had similar problems with the  $R$ ,  $I$ , and  $J$  series, although the afterglow is not detected in these bands. In the  $J$  band there may be a marginal signal in the first epoch (at  $t_0 + 0.19$  days), but this is not significant enough to be measured.

The  $K$ -band light curve displays a prominent brightening during the first day and although this has been observed in a few cases, this is a rare event (Pedersen et al. 1998; Stanek et al. 2007; Guidorzi et al. 2007). There have been a number of explanations for such phenomena ranging from some form of energy injection, dust echoes, and microlensing events to density discontinuities (Tam et al. 2005; Lazzati et al. 2002b).

### 2.2.2. Spectroscopy

On 2007 March 8 (starting at 02:38 UTC) using the VLT UT1/FORS2 instrument with the 300V grism we obtained three spectra with a total exposure time of 5400 s. The spectrum displayed a featureless continuum from 3700 to 9500 Å, apart from a single emission line at  $\sim 9306$  Å. This was attributed to [O II]  $\lambda 3727$  at a redshift of 1.5 on account that no other emission or absorption lines were detected (Jaunsen et al. 2007). The line significance is relatively high, but it is blended with the telluric skylines at 9306 Å and onward, and with a resolution of about 12 Å, this prevented the line from being unambiguously identified. We have considered other potential line identifications such as  $H\beta$ , [O III]  $\lambda 5007$ , or  $H\alpha$ , all of which are rejected on account that we expect to see additional and roughly similar bright lines in the wavelength range 6900–7140 Å.

In an attempt to resolve the [O II] doublet (expected line separation is 7 Å), we observed the host galaxy with the 1028z grism as part of our large program 177.A-0491(J) (PI: Hjorth). The observations were carried out in service mode on 2007 May 7 using VLT FORS2 with a total exposure time of 2600 s. The seeing was 0.7", and sky transparency was clear. The spectra were processed with special emphasis on obtaining a good sky subtraction. The issue is the fact that the skylines in these spectra are somewhat tilted, i.e., not perfectly aligned with the  $y$ -axis. In a traditional reduction the frames are first wavelength-calibrated, which involves an interpolation of the original data values, and then sky-subtracted. Since the steep flanks of the skylines are not sufficiently well sampled, the detailed shapes of the skylines in the interpolated frames vary from row to row, leading to systematic residuals in the sky-subtracted frames. We dealt with this problem by using the method of Kelson (2003) as implemented in Milvang-Jensen et al. (2008).

Since we are only interested in the limited region around the emission line, we manually inspected and cleaned cosmic rays only around the line itself. A cosmic ray on the peak of the emission line of the first spectrum was cleaned by interpolating over the neighboring pixels. A new wavelength solution was obtained by identifying the numerous sky lines throughout the spectrum. The identification of sky lines was done using the UVES sky atlas (Hanuschik 2003). Finally, the new wavelength solution was applied to the stacked sky-subtracted spectrum.

The line-spread function (LSF) is estimated from the sky lines, giving FWHM  $\sim 2.5$  Å, while the detected emission covers approximately 20 Å from 9295 to 9315 Å. If the emission line is due to the [O II] doublet, then a peak to peak separation of nearly 7 Å is expected at this redshift. We fit a Gaussian function to the blue component of the doublet with a fixed width corresponding to the LSF. The red component, which is severely affected by the skyline residuals, is assumed to be 30% brighter than the blue component and separated by 7 Å. Figure 4 shows the spectrum of the doublet with the profiles representing the unperturbed emission lines. The red component of the [O II] doublet (vacuum rest-frame wavelengths  $\lambda 3727.09$ ,  $\lambda 3729.88$ ) is observed at wavelength  $9302.6 \pm 0.2$  Å, which corresponds to a redshift of  $z = 1.49594 \pm 0.00006$ .

The flux-calibrated 300V spectrum was normalized to the  $R$ -band photometry. The integrated flux of the emission line was measured to be  $(1.3 \pm 0.2) \times 10^{-16}$  ergs s $^{-1}$  cm $^{-2}$ . As this emission is significantly affected by the sky line residuals, we use our simple model to estimate a correction factor of 1.3 (by taking the ratio of the model and the spectrum). This is used to estimate the true flux of the [O II] doublet, which becomes  $f_{[\text{O II}],\text{obs}} = (1.7 \pm 0.6) \times 10^{-16}$  ergs s $^{-1}$  cm $^{-2}$ . Note that due to the uncertainty in the flux correction we have added a systematic error. The star formation rate (SFR) can be computed using the relation to [O II] luminosity given by (Kennicutt (1998, eq. [3]),

$$\text{SFR}_{[\text{O II}]} = (1.4 \pm 0.4) \times 10^{-41} L_{[\text{O II}]} M_{\odot} \text{ yr}^{-1} = 34_{-18}^{+25} M_{\odot} \text{ yr}^{-1},$$

where  $L_{[\text{O II}]} = 4\pi d_l^2 f_{[\text{O II}],\text{obs}}$  and  $d_l$  is the luminosity distance.

### 3. THE HOST GALAXY

With an almost featureless optical spectrum, the host galaxy at first seems difficult to model. In the optical we have no indication of an afterglow contribution (variability) and the magnitudes are therefore taken as measurements of the host. The late time NIR photometry is also interpreted as a measure of the NIR host properties. This gives a total of 10 independent magnitudes; SDSS/*ugriz*, FORS/*R*, NOT/*I*, and LIRIS/*JHK*. The adopted host magnitudes are listed in Table 2.

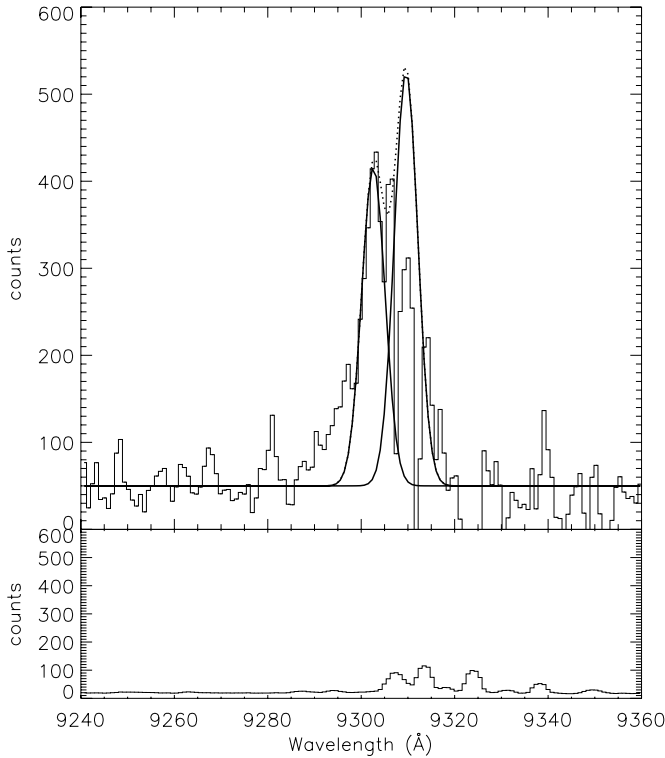


FIG. 4.—[O II] doublet  $\lambda\lambda 3726.1, 3728.8$  at  $z = 1.4959$  of GRB 070306 observed on 2007 May 7 using the VLT FORS2 1028z grism. The red component is affected by skyline residuals in the 9306–9324 Å wavelength range and this is evident when comparing the spectrum to the prominent features in error spectrum. A Gaussian function with the same width as the LSF was fit to the blue component, and the red component was assumed to be 30% brighter than the red and the peaks separated by 7 Å. The result is shown by the solid lines and the combined profile by the dotted line.

The optical colors are consistent with the featureless spectrum, in that they seem to represent a nearly flat continuum. This trend does not continue at the very red end of the spectrum and in the NIR bands. The SDSS  $z$  band deviates from the other bluer bands, although with a large error, and the emission in the NIR peaks in the  $H$  band. We investigate the SED properties by exploring the possible significance of typical emission lines such as  $H\alpha$ ,  $H\beta$ , [O II], and [O III]. The emission-line strengths depend primarily on starburst activity (star formation rate), the age of the stellar population, extinction, and metallicity. The host SED is modeled using the new<sup>9</sup> Hyper-Z (ver. 11; Bolzonella et al. 2000) along with four spectral synthesis models based on Coleman et al. (1980) and two empirical templates Kinney et al. (1996). The Hyper-Z code convolves the templates with the filter transmission curves to obtain colors which are compared to those observed by means of a minimum  $\chi^2$ . This provides some constraint on the host extinction, qualitative information on the SED and an independent

<sup>9</sup> See <http://www.ast.obs-mip.fr/users/rosier/hyperz>.

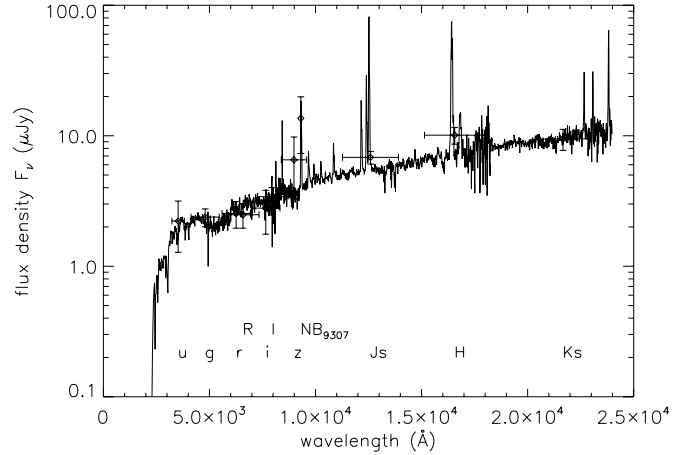


FIG. 5.—Best-fitting SED ( $\chi^2 = 2.5/10$ ) using Hyper-Z and a Kinney et al. (1996) type SB2 template at redshift  $z = 1.50$  with a MW-type extinction curve (Seaton 1979) and  $A_V = 0.17$ . The fit is based on 10 optical and NIR broadband filters and an additional pseudo narrowband filter NB<sub>9307</sub>.

constraint on the redshift (which for this reason is left as a free parameter). The Coleman et al. templates lack detailed emission features, so the Kinney et al. (1996) starburst templates (SB1, SB2) are crucial in order to check their relevance in explaining the observed SED. The difference between the two Kinney et al. (1996) templates is primarily the amount of internal extinction. For the SB1 template  $E(B - V) < 0.1$  and for SB2  $0.11 < E(B - V) < 0.21$ . A satisfactory fit was achieved for all extinction curves we explored, but the MW (Seaton 1979, hereafter S79) curve gave the best result with the Kinney et al. (1996) SB2 template and a relatively well constrained redshift  $z = 1.55^{+0.17}_{-0.26}$  and a  $\chi^2/\text{dof} = 2.3/9$ . The  $\chi^2$  values were all admittedly low, probably suggestive of the errors being large (possibly due to the SDSS errors).

From the spectroscopic results we have a firm constraint on the emission line, and this can be implemented in the SED fitting as a pseudo narrowband measurement at the wavelength of the detected emission line. The NB<sub>9307</sub> filter has an effective wavelength of 9307.5 Å and a 19 Å bandpass. The flux of the NB<sub>9307</sub> filter was determined from the flux-calibrated spectrum, giving NB<sub>9307</sub> =  $21.1 \pm 0.5$  mag (AB). Running Hyper-Z on the 11 magnitude values resulted in a best-fit redshift of  $z = 1.50 \pm 0.01$  and  $\chi^2/\text{dof} = 2.5/10$  and the same combination of the MW (S79) extinction curve and SB2 template. The resulting SED is shown in Figure 5. We thus conclude that the redshift of the host of GRB 070306 is  $z = 1.4959$ , as deduced from spectroscopy. Results from the host SED fits are summarized in Table 3.

The broadband photometry fits to the SED templates do not indicate significant reddening. For the various extinction laws we find the upper limit of  $A_V$  in the range 0.1–0.5. For the best-fitting (SB2) template we find an upper limit of  $A_V \leq 0.45$ .

At the host redshift the [O II] emission occurs in the range  $\lambda\lambda 9304$ – $9310$ , near the edge of the 1028z and 300V grisms. The emission line of [Ne III] is expected at 9660 Å at this redshift,

TABLE 2  
HOST MAGNITUDES

Magnitude	$u$	$g$	$r$	$i$	$z$	$R$	$I$	NB <sub>9307</sub>	$J$	$H$	$K$
Mag (AB).....	23.17	23.06	22.96	22.84	21.90	22.98	22.62	21.1	21.84	21.41	21.47
Error .....	0.46	0.17	0.25	0.40	0.54	0.23	0.19	0.5	0.12	0.16	0.20

NOTE.—The SDSS  $ugriz$  colors are provided by Cool et al. (2007). See § 3 for a description of the pseudo narrowband NB<sub>9307</sub>.

TABLE 3  
RESULTS FROM THE GRB 070306 HOST GALAXY SED FIT OF 10 BROADBAND FILTERS AND ONE PSEUDO NARROWBAND FILTER USING HYPER-Z

Extinction Law	SED	$z$	$\chi^2_\nu$	$A_V$	$\max(A_V)^a$	$z_{\text{low}}$	$z_{\text{up}}$
MW (Allen 1976).....	SB2	1.49	0.256	0.17	0.43	1.49	1.51
MW (Seaton 1979; Fitzpatrick 1986).....	SB2	1.50	0.249	0.17	0.45	1.49	1.51
LMC (Fitzpatrick 1986).....	SB2	1.49	0.268	0.17	0.45	1.48	1.51
SMC (Prevot et al. 1984; Bouchet et al. 1985).....	SB1	1.49	0.316	0.03	0.23	1.48	1.51
SB (Calzetti et al. 2000).....	SB2	1.49	0.269	0.23	0.47	1.48	1.51
SMC (Pei 1992).....	SB1	1.49	0.325	0.00	0.08	1.48	1.51

NOTES.—The extinction curves used here correspond to those implemented in Hyper-Z, in addition to Pei (1992) for the Small Magellanic Cloud (SMC); Allen (1976) for the Milky Way (MW), Seaton (1979) fit by Fitzpatrick (1986) for the MW, Fitzpatrick (1986) for the Large Magellanic Cloud (LMC), Prevot et al. (1984) and Bouchet et al. (1985) for the SMC, and Calzetti et al. (2000) for starburst galaxies (SB).

<sup>a</sup> The (1  $\sigma$ ) upper limit of  $A_V$ .

but unfortunately falls outside the range of both grisms. The best option to independently verify the host redshift is therefore to obtain low resolution spectroscopy in  $J$  and  $H$  bands to search for the [O III],  $H\beta$  and  $H\alpha$  emission lines.

Our best-fitting SED template is a starburst galaxy template. This is typical among GRB host galaxies (Christensen et al. 2004). The UV continuum flux in a starburst galaxy is dominated by the young (bursting) star population, and hence an appropriate measure of the star formation rate. We compute the SFR from the rest-frame UV flux at 2800 Å. The UV flux density is measured at the observed  $2800(1+z)$  Å wavelength in the flux-calibrated spectrum and gives  $f_{2800,\text{obs}} = 3.0 \pm 0.2 \mu\text{Jy}$ , which corresponds to  $L_\nu = 4\pi d_l^2 f_{2800,\text{obs}} / (1+z) = (17.1 \pm 1.2) \times 10^{28} \text{ ergs s}^{-1} \text{ Hz}^{-1}$ . Using Kennicutt (1998, eq. [1]), which relates the SFR to the luminosity at  $\lambda 2800$ , we obtain  $\text{SFR}_{2800} = 24 \pm 2 M_\odot \text{ yr}^{-1}$ . The error on the SFR does not include the roughly 30% error of the Kennicutt relation. The normalized luminosity  $L/L^*$  is estimated from the rest-frame absolute  $B$  magnitude,  $M_B = -22.3$ , which is computed by Hyper-Z. Adopting  $M^* = -21.0$  as the characteristic luminosity of field galaxies, we find a normalized luminosity for the host of  $L/L^* = 3.3$ . This is bright in comparison to other GRB hosts, which primarily are subluminal ( $L < L^*$ ) galaxies (e.g., Fruchter et al. 2006). The luminosity-weighted star formation rate =  $7.3 M_\odot \text{ yr}^{-1} (L/L^*)^{-1}$ . A similar UV estimate at a rest-frame wavelength of 1500 Å can be computed using Madau et al. (1998) and the observed flux density  $f_{1500,\text{obs}} = 1.8 \pm 0.6 \mu\text{Jy}$ . This gives  $L_\nu = (10.3 \pm 3.5) \times 10^{28} \text{ ergs s}^{-1} \text{ Hz}^{-1}$  and an  $\text{SFR}_{1500} = 14.4 \pm 4.9 M_\odot \text{ yr}^{-1}$ .

These SFR estimates are consistent with each other (bearing in mind the 30% uncertainty of the SFR relation) and with the SFR([O II]) computed in § 2.2.2. However, the SFR values are

higher than most of the GRB host galaxies studied in, e.g., Christensen et al. (2004).

#### 4. AFTERGLOW AND EXTINCTION

Variability in GRB 070306 was established early on thanks to the WHT LIRIS data, where a brightening in the  $K$  band of a factor of 2 was detected during the first night (Rol et al. 2007a; Levan et al. 2007). Further observations using VLT ISAAC on the following two nights confirmed the  $K$ -band variability, and revealed variability in the  $H$  band. The complete  $JHK$  light curve is shown in Figure 1. The variability of the afterglow component is most dramatic in the  $K$  band and less pronounced in the  $H$  band. In the  $J$  band only marginal variability, if any at all, is visible during the first night. An afterglow was thus detected in the  $H$  and  $K$  bands during the first three nights.

As described in § 2.2.1 we have used image subtraction to measure the afterglow flux, and if undetected set upper limits to its contribution. To establish the SED of the afterglow, we computed the semisimultaneous flux of the afterglow based on the observations carried out on the second night between 2007 March 08.054 and 08.070 UT. The ISAAC data in this period are superior in quality and therefore best suited for a contemporaneous SED analysis in addition to the FORS  $R$ -band observation at March 08.104 to characterize the SED. We used the AB-offsets calculated by Hyper-Z for the  $R, I, J, H$ , and  $K$  filters and found the values 0.23, 0.45, 0.94, 1.41, and 1.87, respectively. With an afterglow detection in only two bands and two additional upper limits, there is a clear degeneracy in estimating the extinction and spectral slope. We need to introduce constraints on the spectral index, and one option is to assume that the optical spectral index is identical to the X-ray, i.e.,  $\beta_o = \beta_x$ . We fit a number of extinction curves (see

TABLE 4  
REST-FRAME  $A_V$  AND  $\chi^2$  (dof = 1) RESULTS FROM FITTING THE AFTERGLOW SED FOR VARIOUS EXTINCTION CURVES

EXTINCTION LAW	POWER LAW		BROKEN POWER LAW	
	$A_V$	$\chi^2$	$A_V$	$\chi^2$
MW (Allen 1976).....	4.81	0.17	5.31	0.27
MW (Seaton 1979; Fitzpatrick 1986).....	4.81	0.17	5.31	0.27
LMC (Fitzpatrick 1986).....	4.81	0.17	5.31	0.27
SMC (Prevot et al. 1984; Bouchet et al. 1985).....	6.00	0.65	6.71	1.13
SB (Calzetti et al. 2000).....	5.15	0.48	5.75	0.81
SMC (Pei 1992).....	4.93	0.17	5.45	0.26

NOTES.—While the MW and LMC curves provided similar results, the overall best-fitting curve was the SMC curve of Pei (1992). The data are not consistent with the (single) power-law model, except in the case of the SMC curve of Prevot et al. (1984) and Bouchet et al. (1985), where a marginal consistency could be achieved.

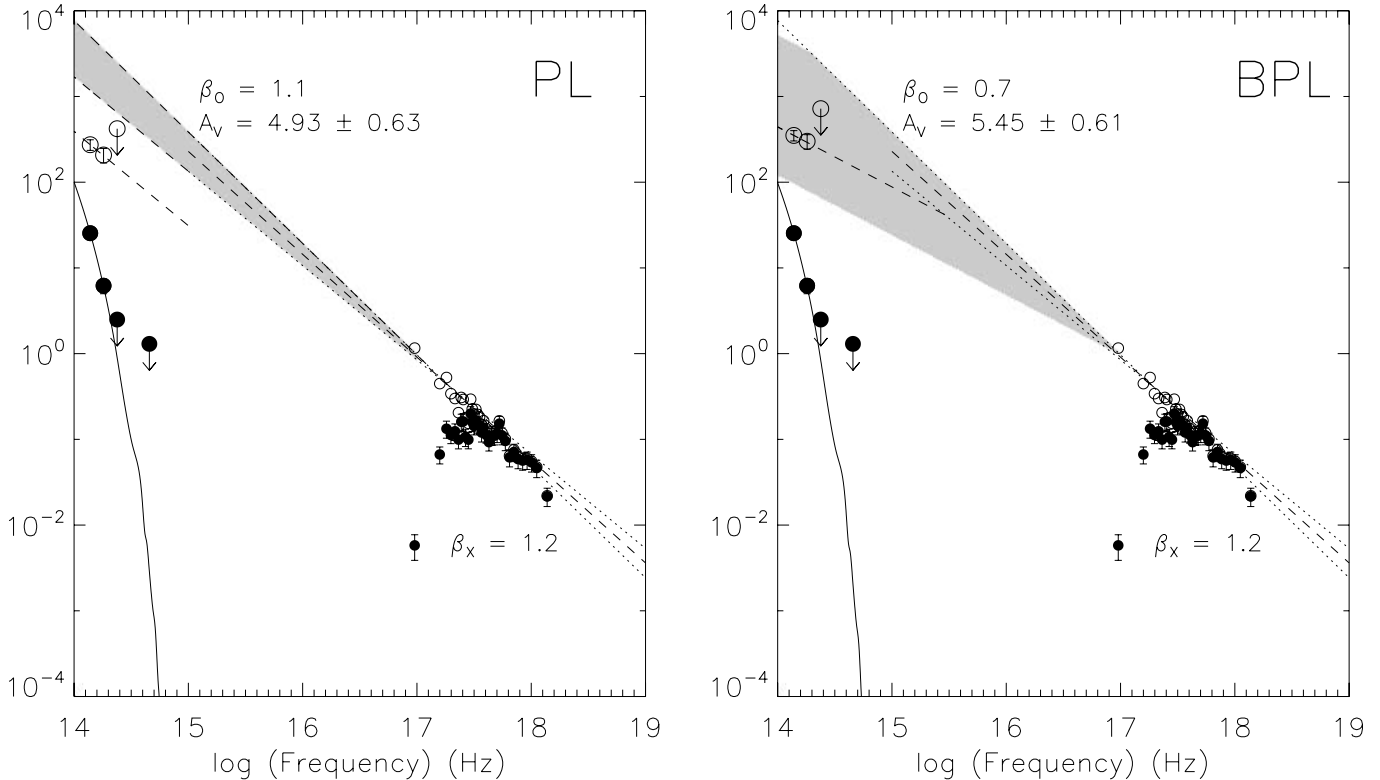


FIG. 6.—Various extinction curves are fit to the optical and NIR afterglow measurements at  $t_0 + 1.38$  days by assuming synchrotron emission in the form of a single-power-law (PL) or broken-power-law (BPL) spectral slope. A separate power-law fit to the XRT data gave a spectral slope of  $\beta_x = 1.2 \pm 0.1$ , which is used to constrain the optical/NIR slope,  $\beta_0$ . The best fit is obtained using the SMC extinction curve of Pei (1992; represented by the rest-frame visual extinction,  $A_V$ ). The observed optical/NIR measurements are shown as large filled circles, whereas the large open circles represent the same data corrected for the best-fit extinction. The small filled dots with error bars represent the XRT data corrected for a fixed Galactic absorption, while the small open dots represent the same data corrected for a variable equivalent hydrogen column density. The shaded areas represent the limits on the total extinction without assuming an extinction curve (see text). The single-power-law model (left) is not consistent with the data for this Pei (1992) SMC curve, but it is marginally consistent using the Prevot et al. (1984); Bouchet et al. (1985) SMC curve.

Table 3) to the broadband optical/NIR data and compare the fits in terms of  $\chi^2$  (see Table 4). The fit is made by assuming an intrinsic (unobscured) spectral slope and fitting the amount of reddening ( $A_V$ ) required such that the corrected points match the assumed spectral slope. The resulting  $A_V$  values are very similar and mostly consistent with each other within the errors. It is difficult to discriminate between the various extinction curves and the MW and LMC curves give the same results, but the SMC extinction curve of Pei (1992) ( $R_V = 2.93$ ) does provide a slightly better fit than the others. By requiring that the NIR slope matches the hardest X-ray slope ( $\beta_0 = 1.1$ ), we obtain an  $A_V = 4.9 \pm 0.6$ . However, the extinction corrected  $H$  and  $K$  points do not match the extrapolation of the X-ray power law, and a single-power-law model is therefore excluded by this fit. If the errors are increased by a factor of 3, then a marginally consistent result can be achieved. The only extinction curve which does allow for the power-law model to succeed is the Pei (1992) SMC-type curve. In the context of the synchrotron model, there is an additional possibility for the optical/X-ray spectrum, namely, a broken power law with the cooling break between the two bands. This requires that  $\beta_0 = \beta_x - 0.5$  and gives a spectral slope of  $\beta_0 = 0.7 \pm 0.1$  using the  $\beta_x$  value from § 2.1. The best-fitting extinction curve is obtained using  $A_V = 5.4 \pm 0.6$ . The errors represent the uncertainty related to the observational errors, which are dominated by the uncertainty of the  $H - K$  color. The SED and extinction curve fits are shown in Figure 6.

The constraints on the total extinction,  $A_\lambda$ , where determined by exploring the possible X-ray spectral slopes and cooling break locations under the assumption that one of the two power-law

models is correct. In the case of a single power law we require that the extinction is not less than the shallowest X-ray slope supported by the data, i.e.,  $\beta > 1.1$ . Similarly, for the broken-power-law model we use the maximum possible cooling break frequency to determine the minimum total extinction. The maximum total extinction comes from the limit of the minimum cooling break frequency, which is set by the frequency of the bluest band with an optical/NIR afterglow detection (e.g., the  $H$  band). The results are given in Table 5 and are visually indicated by the shaded regions in Figure 6.

## 5. SUMMARY AND DISCUSSION

The observational data of GRB 070306 presented here suggest that this is a dark burst with a very red NIR afterglow and that the host ( $z = 1.4959$ ) is brighter than typical host galaxies (Berger et al. 2007). The host of GRB 070306 possesses a higher than normal star formation activity in comparison to other GRB hosts. The afterglow SED analysis shows that significant reddening is

TABLE 5  
TOTAL EXTINCTION CONSTRAINTS

FILTER	POWER LAW		BROKEN POWER LAW	
	min( $A_\lambda$ )	max( $A_\lambda$ )	min( $A_\lambda$ )	max( $A_\lambda$ )
$R$ .....	6.0	...	3.8	...
$J$ .....	6.0	...	4.4	...
$H$ .....	5.4	6.9	2.8	6.9
$K$ .....	4.2	5.7	1.5	5.6

required to explain the observed optical/NIR afterglow assuming typical power laws between the optical/NIR and X-rays. From the combined constraints of the X-ray and optical/NIR data and the assumption of a single or broken power law, we can set limits on the total extinction without requiring a specific extinction law. We find that a single power law is not supported by the data for most of the extinction laws explored, while a broken power law and  $A_V = 5.4 \pm 0.6$  (SMC; Pei 1992) best describes the observed colors.

The Galactic gas-to-dust ratio (Predehl & Schmitt 1995) corresponds to  $N_H = 1.7 \times 10^{21} \times \text{cm}^{-2}/A_V$  (calibrated using X-ray absorption). Using the same ratio, the observed X-ray  $N_H$  would correspond to  $A_V = 15$ , which is much larger than observed, indicating a lower dust-to-gas ratio. Similar results have been found in the past, attributing the apparent deficit to dust destruction, dust depletion, or an unusual ISM composition (Galama & Wijers 2001; Watson et al. 2006; Campana et al. 2007).

In the case of GRB 070306, the combination of what seems to be a highly obscured (and reddened) afterglow and a host with little or no indication of reddening illustrates the general concept that GRB progenitors reside in particularly dense regions within their host galaxies. If, by chance, the GRB line of sight traverses large columns of dust and gas while the host itself appears unobscured, this suggests the dust is unevenly distributed and likely concentrated in smaller regions or clouds within the host galaxy. Such patchy patterns are in effect also seen in our own Galaxy, although it does not necessarily imply that dust and gas trace each other. Padoan et al. (2006) find evidence supporting the latter and suggests spatial fluctuations of the dust-to-gas ratio, even on very small scales, exist in the MW. If the dust obscuration occurs in smaller regions with supposedly varying optical depths, this may also have implications on absorption-line studies and the metallicities resulting from them. There are several element abundance studies in the literature indicating dust depletion (e.g., Savaglio & Fall 2004; Watson et al. 2006), but few (if any) cases providing a robust comparison of emission and absorption-line-induced metallicities. Such studies may therefore offer some hope

in providing a better understanding of the isolated and global properties of these galaxies.

Highly extinguished GRB afterglows are rare, although a few discoveries implying dust have been reported in the past (Masetti et al. 2000; Klose et al. 2000) and more recently (Levan et al. 2006; Rol et al. 2007b; Castro-Tirado et al. 2007; Tanvir et al. 2008). Early NIR observations are crucial in detecting the afterglow of dark bursts, and GRB 070306 illustrates the importance of following NIR afterglows with 8–10 m class telescopes. With the increasing number of apparent dust-obscured (very red) afterglows, all of which are classified as dark, we may be nearing an understanding of the fairly large fraction of dark GRBs. The nature of gamma-ray bursts and their association with regions of intense star-formation, and accordingly an abundance of gas and dust, provides a natural dust interpretation for dark bursts within the context of the synchrotron model. Although there are alternative explanations, the dust-related interpretation seems intuitively in line with the observed red color, the range of redshifts, and host properties. An alternative is that the X-ray and optical afterglows have separate physical origins (Perley et al. 2008). As the number of well-observed dark bursts increase, we are likely to discover many more of these systems, and hopefully settle the ambiguities of interpretation.

We would like to thank the referee for a thorough review and helpful suggestions, which no doubt have improved the manuscript. A. O. J. acknowledges support from the Norwegian Research Council. E. R. acknowledges support from STFC. P. M. V. acknowledges the support of the EU under a Marie Curie Intra-European Fellowship, contract MEIF-CT-2006-041363. The Dark Cosmology Centre is funded by the DNRF. The research activities of J. G. are supported by the Spanish Ministry of Science through the programmes ESP2005-07714-C03-03 and AYA2004-01515. A. J. C. T. acknowledges support from A. de Ugarte Postigo and S. B. Pandey.

#### REFERENCES

- Alard, C., & Lupton, R. H. 1998, *ApJ*, 503, 325  
 Allen, C. W. 1976, *Astrophysical Quantities* (3rd ed; London: Athlone)  
 Andersen, M. L., et al. 2000, *A&A*, 364, L54  
 Barthelmy, S. D., et al. 2007, *GCN Circ.*, 6173, 1  
 Berger, E., Fox, D. B., Kulkarni, S. R., Frail, D. A., & Djorgovski, S. G. 2007, *ApJ*, 660, 504  
 Berger, E., et al. 2002, *ApJ*, 581, 981  
 Bertin, E., & Arnouts, S. 1996, *A&AS*, 117, 393  
 Bolzonella, M., Miralles, J.-M., & Pelló, R. 2000, *A&A*, 363, 476  
 Bouchet, P., Lequeux, J., Maurice, E., Prevot, L., & Prevot-Burnichon, M. L. 1985, *A&A*, 149, 330  
 Burrows, D. N., et al. 2005, *Space Sci. Rev.*, 120, 165  
 Calzetti, D., Armus, L., Bohlin, R. C., Kinney, A. L., Koornneef, J., & Storchi-Bergmann, T. 2000, *ApJ*, 533, 682  
 Campana, S., et al. 2007, *ApJ*, 654, L17  
 Castro-Tirado, A. J., et al. 2007, *A&A*, 475, 101  
 Christensen, L., Hjorth, J., & Gorosabel, J. 2004, *A&A*, 425, 913  
 Coleman, G. D., Wu, C.-C., & Weedman, D. W. 1980, *ApJS*, 43, 393  
 Cool, R. J., et al. 2007, *GCN Circ.*, 6170, <http://gcn.gsfc.nasa.gov/gcn/gcn3/6720.gcn3>  
 Dickey, J. M., & Lockman, F. J. 1990, *ARA&A*, 28, 215  
 Fitzpatrick, E. L. 1986, *AJ*, 92, 1068 (F86)  
 Fruchter, A. S. 1999, *ApJ*, 512, L1  
 Fruchter, A. S., et al. 2006, *Nature*, 441, 463  
 Fynbo, J. P. U., Hjorth, J., Malesani, D., Sollerman, J., Watson, D., Jakobsson, P., Gorosabel, J., & Jaunsen, A. O. 2008, in *Proc. Eleventh Marcel Grossmann Meeting on General Relativity*, ed. H. Kleinert, R. T. Jantzen, & R. Ruffini (World Scientific: Singapore), in press  
 Fynbo, J. U., et al. 2001, *A&A*, 369, 373  
 Galama, T. J., & Wijers, R. A. M. J. 2001, *ApJ*, 549, L209  
 Galama, T. J., et al. 1998, *Nature*, 395, 670  
 Gehrels, N., et al. 2004, *ApJ*, 611, 1005  
 Groot, P. J., et al. 1998, *ApJ*, 493, L27  
 Guidorzi, C., et al. 2007, *A&A*, 474, 793  
 Hanuschik, R. W. 2003, *A&A*, 407, 1157  
 Hjorth, J., et al. 2003, *Nature*, 423, 847  
 Jakobsson, P., Hjorth, J., Fynbo, J. P. U., Watson, D., Pedersen, K., Björnsson, G., & Gorosabel, J. 2004, *ApJ*, 617, L21  
 Jaunsen, A. O., Thoene, C. C., Fynbo, J. P. U., Hjorth, J., & Vreeswijk, P. 2007, *GCN Circ.*, 6202, <http://gcn.gsfc.nasa.gov/gcn/gcn3/6921.gcn3>  
 Jester, S., et al. 2005, *AJ*, 130, 873  
 Kelson, D. D. 2003, *PASP*, 115, 688  
 Kennicutt, R. C., Jr. 1998, *ARA&A*, 36, 189  
 Kinney, A. L., Calzetti, D., Bohlin, R. C., McQuade, K., Storchi-Bergmann, T., & Schmitt, H. R. 1996, *ApJ*, 467, 38  
 Klose, S., et al. 2000, *ApJ*, 545, 271  
 Lamb, D. Q., & Reichart, D. E. 2000, *ApJ*, 536, 1  
 Lazzati, D., Covino, S., & Ghisellini, G. 2002a, *MNRAS*, 330, 583  
 Lazzati, D., Rossi, E., Covino, S., Ghisellini, G., & Malesani, D. 2002b, *A&A*, 396, L5  
 Levan, A., et al. 2006, *ApJ*, 647, 471  
 Levan, A., Rol, E., Tanvir, N., Schirmer, M., & Castro-Tirado, A. J. 2007, *GCN Circ.*, 6176, <http://adsabs.harvard.edu/abs/2007GCN..6176....1L>  
 Madau, P., Pozzetti, L., & Dickinson, M. 1998, *ApJ*, 498, 106  
 Malesani, D., Jaunsen, A. O., Thoene, C. C., Hjorth, J., Paraficz, D., Leitert, E., & Caldwell, B. 2007, *GCN Circ.*, 6178, <http://adsabs.harvard.edu/abs/2007GCN..6176....1L>  
 Masetti, N., et al. 2000, *A&A*, 354, 473  
 Milvang-Jensen, B., et al. 2008, *A&A*, 482, 419  
 Padoan, P., Cambrésy, L., Juvela, M., Kritsuk, A., Langer, W. D., & Norman, M. L. 2006, *ApJ*, 649, 807  
 Page, K. L., & Pandey, S. B. 2007, *GCN Circ.*, 6172, <http://gcn.gsfc.nasa.gov/gcn/gcn3/6172.gcn3>

- Pandey, S. B., Barthelmy, S. D., Pasquale, M. D., Page, K. L., & Evans, P. 2007, *GCN Rep.*, 38, 2
- Pedersen, H., et al. 1998, *ApJ*, 496, 311
- Pei, Y. C. 1992, *ApJ*, 395, 130
- Perley, D. A., et al. 2008, *ApJ*, 672, 449
- Predehl, P., & Schmitt, J. H. M. M. 1995, *A&A*, 293, 889
- Prevot, M. L., Lequeux, J., Prevot, L., Maurice, E., & Rocca-Volmerange, B. 1984, *A&A*, 132, 389
- Rol, E., Levan, A., Tanvir, N., Schirmer, M., & Castro-Tirado, A. J. 2007a, *GCN Circ.*, 6174, <http://gcn.gsfc.nasa.gov/gcn/gcn3/6174.gcn3>
- Rol, E., et al. 2007b, *ApJ*, 669, 1098
- Roming, P. W. A., et al. 2006, *ApJ*, 652, 1416
- Savaglio, S., & Fall, S. M. 2004, *ApJ*, 614, 293
- Schlegel, D. J., Finkbeiner, D. P., & Davis, M. 1998, *ApJ*, 500, 525
- Seaton, M. J. 1979, *MNRAS*, 187, 73 (S79)
- Stanek, K. Z., et al. 2007, *ApJ*, 654, L21
- . 2003, *ApJ*, 591, L17
- Tam, P. H., Pun, C. S. J., Huang, Y. F., & Cheng, K. S. 2005, *NewA*, 10, 535
- Tanvir, N. R., et al. 2008, *MNRAS*, submitted (arXiv: 0803.4100T)
- Uemura, M., Arai, A., & Uehara, T. 2007, *GCN Circ.*, 6171, <http://gcn.gsfc.nasa.gov/gcn/gcn3/6171.gcn3>
- Watson, D., et al. 2006, *ApJ*, 652, 1011
- Wijers, R. A. M. J., Bloom, J. S., Bagla, J. S., & Natarajan, P. 1998, *MNRAS*, 294, L13